AD A132597

GENERAL ⊛ ELECTRIC

MILITARY ELECTRONIC SYSTEMS OPERATION

TECHNICAL INFORMATION SERIES

Author John P. Costas	Subject Category Detection Waveform Design	No. R83EMH002
		Date July 1983

Title A STUDY OF A CLASS OF DETECTION WAVEFORMS HAVING NEARLY IDEAL RANGE-DOPPLER AMBIGUITY PROPERTIES		

Copies Available at MESO TIS Distribution Center Box 4840 (CSP 4-18) Syracuse, New York 13221	GE Class 1	No. of Pages
	Govt Class Unclassified	40

Summary
 ⟶ A special class of permutation matrices is considered. It is shown that these matrices may be beneficially used to determine the frequency-time pattern of a uniform pulse train. Proper choice of burst waveform parameters is shown to result in a detection waveform having range and doppler resolution properties consistent with the overall signal duration and bandwidth. The range-doppler sidelobe peaks are well-controlled so that the ideal "thumbtack" ambiguity function behavior is closely approximated by the synthesis procedure presented.

DTIC
ELECTE
SEP 19 1983
S   D

D

Send to __

DTIC FILE COPY

83 09 12 069

GENERAL ELECTRIC COMPANY TECHNICAL INFORMATION

Within the limitations imposed by Government data export regulations and security classifications, the availabil.. of General Electric Company technical information is regulated by the following classifications in order to safeguard proprietary information:

CLASS 1: <u>GENERAL INFORMATION</u>

Available to anyone on request.
Patent, legal and commercial review
required before issue.

CLASS 2: <u>GENERAL COMPANY INFORMATION</u>

Available to any General Electric Company
employee on request.
Available to any General Electric Subsidiary
or Licensee subject to existing agreements.
Disclosure outside General Electric Company
requires approval of originating component.

CLASS 3: <u>LIMITED AVAILABILITY INFORMATION</u>

Original Distribution to those individuals with
specific need for information.
Subsequent Company availability requires
originating component approval.
Disclosure outside General Electric Company
requires approval of originating component.

CLASS 4: <u>HIGHLY RESTRICTED DISTRIBUTION</u>

Original distribution to those individuals person-
ally responsible for the Company's interests in
the subject.
Copies serially numbered, assigned and recorded
by name.
Material content, and knowledge of existence,
restricted to copy holder.

GOVERNMENT SECURITY CLASSIFICATIONS, when required, take precedence
in the handling of the material. Wherever not specifically disallowed, the General
Electric classifications should also be included in order to obtain proper handling
routines.

SECTION _____ Advanced Development Engineering _____

UNIT _____ 570 _____

MESO ACCOUNTING REFERENCE _____ 570 _____

COLLABORATORS _____

APPROVED _____ *G. Oehling* _____ TITLE Manager, ADE _____ LOCATION _____ CSP 4-5 _____

MINIMUM DISTRIBUTION - Government Unclassified Material (and Title Pages) in G.E. Classes 1, 2, or 3 will be the following.

Copies	Title Page Only	To
0	1	Legal Section, MESO (Syracuse)
0	1	Manager, Technological Planning, MESO (Syracuse)
5	6	G-E Technical Data Center (Schenectady)

MINIMUM DISTRIBUTION - Government Classified Material, Secret or Confidential in G.E. Classes 1, 2, or 3 will be the following.

1	0	Manager, Technological Planning, MESO (Syracuse)

ADDITIONAL DISTRIBUTION (Keep at minimum within intent of assigned G.E. Class.)

COPIES	NAME	LOCATION
5 (CLASS 1 ONLY)	DEFENSE DOCUMENTATION CENTER	CAMERON STATION, ALEXANDRIA, VA. 22314
1	L.I. Chasen	P.O. Box 8555 Philadelphia, Pa., 19101
1	S.B. Akers, Jr.	CSP 4-5, Syracuse, NY 13221
1	S.P. Applebaum	CSP 4-38A, Syracuse, NY 13221
1	L.W. Bauer	Bldg 37, Rm 525, Schenectady, NY 12345
1	R.L. Benfey	CSP 5-4C, Syracuse, NY 13221
1	H.H. Burkart	FRP 1-F2, Syracuse, NY 13221
1	Prof. G.R. Cooper	School of Electrical Engineering, West Lafayette, Indiana 47907
1	J.A. Edward	FRP 1-J7, Syracuse, NY 13221
1	W.I. Fenster	CSP 5-J1, Syracuse, NY 13221
1	M.M. Fitelson	FRP 1-10B, Syracuse, NY 13221
1	E.P. Gasparek	CSP 4-57, Syracuse, NY 13221
1	B.H. Geyer, Jr.	CSP 5-6G, Syracuse, NY 13221
1	R.E. Girmus	FRP 1-R7, Syracuse, NY 13221
1	Prof. S.W. Golomb	University of So. California, Powell Hall, University Park, Los Angeles CA 90089
1	Dr. P.E. Green, Jr.	International Business Machines Corp, Armonk, NY 10504
1	R. Janer	FRP 1-D6, Syracuse, NY 13221
1	M.A. Johnson	CSP 4-58, Syracuse, NY 13221

Copies	Name	Location
1	R. R. Kinsey	CSP 4-57, Syracuse, NY 13221
1	D. H. Kuhn	CSP 4-57, Syracuse, NY 13221
1	J. P. Kuhn	FRP 1-J7, Syracuse, NY 13221
1	J. P. Lindhuber	FRP 1-J7, Syracuse, NY 13221
1	C. E. Nelson	CSP 4-38A, Syracuse, NY 13221
1	R. Nitzberg	CSP 4-5, Syracuse, NY 13221
1	G. Oehling	CSP 4-58, Syracuse, NY 13221
1	K. A. Olsen	CSP 4-41, Syracuse, NY 13221
1	G. Otteni	CSP 4-57, Syracuse, NY 13221
1	J. R. Pratt	FRP 1-J7, Syracuse, NY 13221
1	Dr. R. Price	Sperry Research Center, 100 North Rd., Sudbury, MA 01776
1	J. G. Reddeck	CSP 4-5, Syracuse, NY 13221
1	J. A. Rougas	CSP 4-4, Syracuse, NY 13221
1	R. W. Scharstein	CSP 4-57, Syracuse, NY 13221
1	F. D. Shapiro	FRP 1-R5, Syracuse, NY 13221
1	T. B. Shields	CSP 5-7K, Syracuse, NY 13221
1	O. H. Shuart	CSP 3-2, Syracuse, NY 13221
1	J. Slocum	CSP 4-4, Syracuse, NY 13221
1	L. J. Spafford	CSP 4-41, Syracuse, NY 13221
1	J. W. Stauffer	FRP 1-J7, Syracuse, NY 13221
1	C. A. Stutt	Bldg 5, Rm. 209, Schenectady, NY 12345
1	R. W. Swanson	CSP 1-8, Syracuse, NY 13221
1	B. W. Tietjen	FRP 1-F2, Syracuse, NY 13221
1	E. M. Valovage	FRP 1-J7, Syracuse, NY 13221
1	M. J. Viggiano	CSP 4-57, Syracuse, NY 13221
1	B. P. Viglietta	CSP 4-57, Syracuse, NY 13221
1	A. M. Vural	FRP 1-J7, Syracuse, NY 13221
1	L. F. Waful	FRP 1-F2, Syracuse, NY 13221
1	R. Wasiewicz	CSP 4-5, Syracuse, NY 13221
1	Prof. L. R. Welch	University of So. California, EE Dept, PHE-Rm 502, Los Angeles, CA 90089-0272
1	D. W. Winfield	FRP 1-J7, Syracuse, NY 13221
1	W. P. Whyland	FRP 1-J7, Syracuse, NY 13221

TABLE OF CONTENTS

LIST OF ILLUSTRATIONS

INTRODUCTION

This paper considers the coherent processing of detection waveforms having the form of frequency-hopped uniform pulse trains. It is shown that if the parameters of the pulse train are properly chosen, the range and doppler responses will be unambiguous, and will be consistent with the overall burst duration and bandwidth, respectively. It is further demonstrated that very well-behaved range-doppler sidelobes will be obtained if the frequency schedule or "firing order" is derived from a class of permutation matrices having special properties.

It might be of some interest to note that the basic concept demonstrated here came from an application area in which fully-coherent processing was found to be inappropriate. In a discussion of this prior work with Dr. P.E. Green, Jr. of IBM, it was suggested that an extension of scope to include the fully coherent signal processor might prove useful. This paper is the direct result of Dr. Green's comments.

A SPECIAL CLASS OF PERMUTATION MATRICES

In a study of long-range active sonar systems it was found that time-varying multipath "medium effects" could seriously limit the performance of high TW-product, fully coherent systems [1]. The medium-spreading effects are not unlike those encountered by Price and Green [2] in radio astronomy work. The medium spread factors encountered in the sonar case suggested use of a hybrid coherent/noncoherent technique. Simple CW pulses are transmitted in the available time-frequency space. The receiver employs a bank of filters whose outputs are individually detected. A delay-and-add matrix is then used for the generation of echo amplitude vs range outputs for a set of assumed target-doppler values. The filter bank provides the coherent processing, while the detectors and the delay-and-add matrix perform a non-coherent addition function in the hybrid receiver/processor.

The problem of choosing the frequency-hopping pattern for the burst is influenced by several factors: Under peak-power limitations energy per pulse will be maximized if only one pulse is transmitted at any one time. Energy per pulse is a key parameter of the detection process under noise-limited conditions. Under reverberation (clutter) - limited conditions a self-jamming situation exists so that independent "looks" at the target are needed to enhance detection performance. For example, a second pulse placed in a frequency channel will be wasted since the doubling of the echo energy is negated by a doubling of the background (reverberation) level. Hence only one pulse should appear in each frequency channel of the transmit burst if performance in reverberation (clutter) is to be optimized.

Having established the one pulse per time period and one pulse per frequency channel rule, there still remains the problem of the range-doppler ambiguity in selecting firing order. The classic frequency staircase or quantized FM (QFM) pattern, for example, is a very poor choice from an ambiguity standpoint. In an NxN frequency-time array there are N! patterns that satisfy the "one-and-one" condition; how does one select "good" patterns?

We invoke first the narrowband assumption which implies that target doppler will shift all echoes by the same amount. [This is definitely not valid in most sonar applications, but the patterns which result using the narrowband assumption perform surprisingly well under the actual (broadband) operating conditions.] The ambiguity problem arises from the fact that the receiver operates as a two-dimensional coincidence detector. For example, when N pulses arrive having the frequency and time positions of the transmit pattern (zero-doppler target), these N pulses are detected, delayed and combined to given an N-value response out

of the zero-doppler processor. Consider now that a second (moving) target is also present. A frequency-shifted echo pattern from this target will result. If this second frequency-shifted pattern has K coincidences with the zero-doppler pattern for some relative time shift, the zero-doppler processor will give a K-value response to this echo. The value K may not be made zero for all time and frequency shifts but can it be constrained to unit level?

The problem can now be very simply stated: Place N ones in an otherwise null N by N matrix such that each row contains a single one as does each column. Make the placement such that for all possible x-y shift combinations of the resulting (permutation) matrix relative to itself, at most one pair of ones will coincide.

In spite of the geometric simplicity of the problem statement, early efforts toward a solution either failed or gave very limited results. A few mathematicians were contacted with absolutely no results. A computer program which did a random search for ideal patterns failed miserably until the threshold was raised above the ideal level. The program then gave some useful patterns which satisfied the engineering needs of the moment. However, questions concerning the ideal patterns remained largely unanswered.

It was realized early on that an alternate statement of the problem could be made: Order the complete set of integers from 1 to N such that the difference triangle formed from the ordered sequence shall have no repeated terms in any row. That is, form the first row by taking differences between adjacent numbers. All differences in this row must be unique. Form the second row by taking differences between next-adjacent terms. This row must also be free of repeated values, and so forth. A simple example of this process is shown in Table 1 for N = 10. In the table L represents the order of the difference, $\left\{\theta_m\right\}$ the ordered integer set.

TABLE 1

DIFFERENCE TRIANGLE FOR N = 10

L \ $\left\{\theta_m\right\}$	2	4	8	5	10	9	7	3	6	1
1	2	4	-3	5	-1	-2	-4	3	-5	
2	6	1	2	4	-3	-6	-1	-2		
3	3	6	1	2	-7	-3	-6			
4	8	5	-1	-2	-4	-8				
5	7	3	-5	1	-9					
6	5	-1	-2	-4						
7	1	2	-7							
8	4	-3								
9	-1									

Using the difference triangle method, ideal sequences were found for all N up to 12. N = 13, however, always remained beyond my pencil-and-paper grasp. Realization that the problem could be stated in terms of the ordered integer set convinced me that this was a problem of antiquity. With this in mind, Professor Solomon W. Golomb was contacted, a short summary of the problem and work to date was given, and references concerning sequences having the stated property were requested.

Golomb's prompt reply was notable for two main reasons: First, he stated that no reference could be given as this was apparently a new problem. Secondly, he offered me a series of conjectures that have proven quite accurate. Golomb believed that solutions existed for all N, that the number of solutions would grow very rapidly with N, and that the density of solutions would become very small as N became large. Notable progress has since been made by Golomb, Taylor, Welch and Lempel. Some of their results may be found in a recent [3] and a pending [4] publication.

All known systematic constructions for these arrays involve the use of primitive elements of finite fields. A very elegant and simple construction method is given in a theorem by L.R. Welch [4]:

"Let g be a primitive root modulo the prime p. Then the (p-1) x (p-1) permutation matrix with a_{ij} = 1 iff $j \equiv g^i$ (mod p), $1 \leq i \leq p-1$, $1 \leq j \leq p-1$ is a Costas array."

The difference triangle example of Table 1 made use of Welch's theorem for p = 11, g = 2. Note that 2 raised to succeeding powers (modulo 11) will yield the ordered integer set shown in the example. Armed with the new knowledge that the density of solutions is small (relative to the number of possible permutation matrices, N!), the writer developed computer programs which do an ordered, exhaustive search for these arrays. These programs have produced solutions for N = 19 for which there are no known algebraic constructions. Also the programs have shown that the number of solutions for N = 3, 4, ----12 are: 4, 12, 40, 116, 200, 444, 760, 2160, 4368 and 7852 respectively.

Unfortunately the fastest algorithm available becomes useless for N values much above 20. At one time there was no known construction for N = 24. A computer search for this N was started many months ago which has yet to finish. Several hundred VAX* 11/780 processor hours are estimated to have been expended to date on a weekends-only, slow-queue, lowest-priority basis. In the meantime an algebraic construction for N = 24 has been discovered and the VAX* search has been abandoned.

---

*VAX is a trademark of the Digital Equipment Corporation.

In the sections which follow two arrays based on Welch's theorem will be used. A "Welch-10" based on $\rho = 11$, $g = 2$ has firing order:

2, 4, 8, 5, 10, 9, 7, 3, 6, 1

and a "Welch-30" based on $p = 31$, $g = 3$ has firing order:

3, 9, 27, 19, 26, 16, 17, 20, 29, 25
13, 8, 24, 10, 30, 28, 22, 4, 12, 5
15, 14, 11, 2, 6, 18, 23, 7, 21, 1

These arrays are used because they are very easy to calculate. There is no reason to believe that other constructions due to Taylor, Lempel, Golomb, or the computer-derived sequences generated by the writer's algorithms would produce significantly different results for the applications which follow.

ANALYSIS OF A SPECIAL CLASS OF BURST WAVEFORMS

It is useful to formalize the difference triangle property associated with this special class of permutation matrices. Let the sequence of ordered integers be represented by

$$\{\theta_n\} = \theta_0, \theta_1, \theta_2, \theta_3, \text{---} \theta_{N-1} \tag{1}$$

The Lth row of the difference triangle will contain terms:

$$\Delta_{L,k} = \theta_{k+L} - \theta_k \tag{2}$$

$$L = 1, 2, \text{--}, N-2; \quad k = 0, 1, 2, \text{---}, N-1 \cdot I,$$

and for every L

$$\Delta_{L,r} \neq \Delta_{L,s} \text{ for } r \neq s \tag{3}$$

A fairly general treatment of pulse trains is given by Rihaczek [5] . We treat here a special case in which N unit envelope CW pulses of duration T appear contiguously to form a burst of overall length NT. The frequency of each pulse will be given by

$$f_n = \frac{\theta_n}{T} \tag{4}$$

where the θ_n are taken from (1). (In the analysis which follows θ_n -1 is actually assumed so that $0 \leq \theta_n \leq N-1$. This unit shift from the Welch theorem results is trivial but convenient.) Note that the time-bandwidth product of the resulting waveform is approximately equal to N^2.

The pulse train $\mu(t)$ will be given by (complex envelope representation)

$$\mu(t) = \sum_{n=0}^{N-1} p_n(t-nT) \tag{5}$$

where

$$p_n(t) = e^{+j2\pi f_n t} \qquad 0 \leq t \leq T \tag{6}$$

$$p_n(t) = 0 \qquad \text{elsewhere}$$

The delay-doppler ambiguity function is defined as

$$\chi(\tau, \nu) = \frac{1}{2E} \int_{-\infty}^{\infty} \mu^*(\sigma) \mu(\sigma - \tau) \, e^{+j2\pi\nu\sigma} \, d\sigma \tag{7}$$

Where E is the total energy of $\mu(t)$. For the example at hand $E = NT/2$ so that

$$\chi(\tau, \nu) = \frac{1}{NT} \int_{-\infty}^{\infty} \mu^*(\sigma) \mu(\sigma - \tau) e^{+j2\pi\nu\sigma} \, d\sigma \tag{8}$$

It is easily proven that

$$\left| \chi(\tau, \nu) \right| \leq 1 = \left| \chi(0,0) \right| \tag{9}$$

and

$$\left| \chi(-\tau, -\nu) \right| = \left| \chi(\tau, \nu) \right| \tag{10}$$

and

$$\int_{-\infty}^{\infty} \int_{-\infty}^{\infty} \left| \chi(\tau, \nu) \right|^2 \, d\tau \, d\nu = 1 \tag{11}$$

For computational purposes advantage was taken of (10) so that only non-negative values of τ are required. The relationship

$$\left. \begin{array}{l} \tau = kT + \delta \\ 0 \leq \delta \leq T, \quad k = 0, 1, 2 \text{ --}, N\text{-}1 \end{array} \right\} \tag{12}$$

was used in conjunction with (6) and (8) to obtain

$$\chi(\tau, \nu) = \sum_{r=0}^{N-1-k} A + \sum_{r=0}^{N-2-k} B \tag{13}$$

where

$$A = \frac{(T - \delta)}{NT} \left[\frac{\sin \pi\beta \, (T - \delta)}{\pi\beta \, (T - \delta)} \right] \times \exp\left\{ j\pi \left[\beta \, (2kT + 2rT + T + \delta) - 2f_r \delta \right] \right\}$$

$$\tag{14}$$

where

$$\beta \triangleq f_r - f_{k+r} + \nu \tag{15}$$

$$B = \frac{\delta}{NT} \left[\frac{\sin \pi \gamma \delta}{\pi \gamma \delta} \right] \times \exp \left\{ j\pi \left[\gamma (2kT + 2rT + 2T + \delta) - 2f_r \delta \right] \right\} \tag{16}$$

and

$$\gamma \triangleq f_r - f_{k+r+1} + \nu \tag{17}$$

The subscripted frequency values conform to (4).

The above approach provided a computational convenience for producing the quantitative data shown in the figures which follow. A different development of (8) will now be undertaken which better demonstrates physical principles. Define the cross-correlation function

$$\phi_{nm} (\tau, \nu) \triangleq \frac{1}{T} \int_{-\infty}^{\infty} p_n^* (\sigma) \, p_m (\sigma - \tau) \, e^{+j2\pi \nu \sigma} d\sigma \tag{18}$$

which with (6) yields

$$\phi_{nm} (\tau, \nu) = \frac{(T - |\tau|)}{T} \frac{\sin \pi a (T - |\tau|)}{\pi a (T - |\tau|)} \times \exp \left[j\pi a (T + \tau) - j2\pi f_m \tau \right] \tag{19}$$

$|\tau| \leq T$, zero elsewhere

$$a = f_n - f_m - \nu \tag{20}$$

The autocorrelation function, ϕ_{nn}, is obtained from (20) setting $m = n$ to obtain

$$\phi_{nn}(\tau, \nu) = \frac{(T - |\tau|)}{T} \frac{\sin \pi \nu (T - |\tau|)}{\pi \nu (T - |\tau|)} \times \exp\left[j\pi\nu (T + \tau) - j2\pi f_n \tau \right] \qquad (21)$$

$|\tau| \leq T$, zero elsewhere.

Using (5), (6) and (8)

$$\chi(\tau, \nu) = \frac{1}{NT} \int_{-\infty}^{\infty} \sum_{n=0}^{N-1} p_n^* (\sigma - nT) \times \sum_{m=0}^{N-1} p_m (\sigma - \tau - mT) \, e^{+j2\pi\nu\sigma} d\sigma \qquad (22)$$

Changing summation and integration orders and grouping summations into like and unlike subscript categories, one obtains

$$\chi(\tau, \nu) = \frac{1}{N} \sum_{n=0}^{N-1} e^{+j2\pi n\nu T} \left[\phi_{nn}(\tau, \nu) + \sum_{\substack{m=0 \\ m \neq n}}^{N-1} \phi_{nm}(\tau - (n-m)T, \nu) \right]$$

$$(23)$$

Note especially that

$$\phi_{nm}(\tau, \nu) = \phi_{nn}(\tau, \nu) = 0$$

$$(24)$$

for $|\tau| \geq T$

The magnitude of $\chi(\tau, \nu)$ represents the magnitude of the coherent processor response to a pulse train arriving with delay τ and frequency or doppler shift ν. We would like a zero response everywhere except for $\tau = 0$, $\nu = 0$. Equation (11) shows that this is not possible. If the main peak of $|\chi|$ is narrow in both τ and ν for good resolution properties, the volume of $|\chi|^2$ under the main peak will be small. The bulk of the volume in such cases will then fall

10

in the "pedestal" or "sidelobe" region of the ambiguity function. Waveform choice to minimize the deleterious effects of the pedestal is an important facet of detection system design. The criteria vary with the application at hand [2,6,7]. In this work we shall try to keep the peak sidelobe values confined.

It will now be shown that the central peak of (23) is associated with the ϕ_{nm} sum while the sidelobe responses may be associated, in the main, with the ϕ_{nm} sum.

Consider first the $\tau = 0$ axis. Note from (24) that all ϕ_{nm} terms are zero here. Then

$$\chi(0, \nu) = \frac{1}{N} \sum_{n=0}^{N-1} e^{+j2\pi n \nu T} \phi_{nn}(0, \nu) \tag{25}$$

Using (21) and the identity

$$\sum_{r=0}^{N-1} e^{jar} = e^{j(N-1)a/2} \frac{\sin N a/2}{\sin a/2} \tag{26}$$

one obtains the exact result

$$\chi(0, \nu) = e^{jN\pi\nu T} \frac{\sin N\pi\nu T}{N\pi\nu T} \tag{27}$$

which shows that the doppler resolution of the N-pulse burst is identical to that of a CW pulse of duration NT.

It is convenient to define a normalized frequency variable y, where

$$y \overset{\Delta}{=} \nu T \tag{28}$$

Since the frequency channel spacing is 1/T, y is in essence a measure of frequency in units of channel spacing. Equation (27) may then be written as

$$\chi(0, y) = e^{j\pi Ny} \frac{\sin \pi Ny}{\pi Ny} \tag{29}$$

The first zero of χ will occur at $y = \pm 1/N$. The half-baseline width of the main lobe, $1/N$, may be considered a measure of system frequency resolution.

The behavior of $\chi (\tau, \nu)$ of (23) along the range axis ($\nu=0$) is complicated by the fact that the ϕ_{nm} (second) summation does contribute to this main axis response, even though it is only the ϕ_{nn} (first) summation that is desired here. Let χ' be that part of (23) which excludes the second sum

$$\chi' (\tau, 0) \overset{\Delta}{=} \frac{1}{N} \sum_{n=0}^{N-1} \phi_{nn} (\tau, 0) \tag{30}$$

Use of (21) yields

$$\chi' (\tau, 0) = \frac{(T - |\tau|)}{NT} \sum_{n=0}^{N-1} e^{-j2\pi f_n \tau} \tag{31}$$

$|\tau| \leq T$, zero elsewhere.

Now f_n is given by (4) in terms of the ordered integer set $\{\theta_n\}$ as per (1). Note however that in (31) a sum over N terms is involved, the order in which the f_n values appear is immaterial. If we decrement each θ_n by 1 then the value n/T may be used for f_n in (31). This yields

$$\chi' (\tau, 0) = \frac{(T - |\tau|)}{T} \sum_{n=0}^{N-1} e^{-j2\pi n \frac{\tau}{T}} \tag{32}$$

Use of the identity (26) gives

$$\chi' (\tau, 0) = \frac{(T - |\tau|)}{T} e^{-j\pi(N-1)\frac{\tau}{T}} \frac{\sin\pi N \tau/T}{N \sin \pi \tau/T} \tag{33}$$

$|\tau| \leq T$, zero elsewhere

The autocorrelation terms of (23) produce a range axis magnitude response that has a unit peak value at $\tau = 0$ and would also peak again at $\tau = T$ were it not for the $(T - |\tau|)$ factor. For the larger N values the $\sin Nz/(N \sin z)$ ratio behaves very much like the $\sin Nz/Nz$ form of (27). It is convenient to define a normalized delay variable as

$$x \triangleq \frac{\tau}{T} \tag{34}$$

Then (33) becomes

$$\chi'(x, 0) = (1 - |x|) \ e^{-j\pi(N-1)x} \ \frac{\sin\pi Nx}{N \sin\pi x} \tag{35}$$

$|x| < 1$, zero elsewhere

For $|x| > 1$ ($|\tau| > T$) like-frequency pulses no longer overlap in the convolution integral of (7) and χ' has zero value here. The τ-axis response beyond $|\tau| = T$ is entirely due to cross-product terms ϕ_{nm} of (23), and in a sense these line regions become part of the pedestal or sidelobe regions.

An examination now begins of the ϕ_{nm} crossproduct terms of (23) which are responsible for the pedestal of the ambiguity surface. Equations (19) and (20) show that the ϕ_{nm} terms will peak to unit value when

$$\left. \begin{array}{l} \tau = \tau_p = (n-m) \ T \\ \\ \nu = \nu_p = f_n - f_m \end{array} \right\} \tag{36}$$

and

Because of central-point symmetry of the χ function only positive delay values need be considered. The range of (n-m) of (36) will be 1 to N-1. So that

$$\tau_p = LT, \ L = 1, \ 2, ---(N-1) \tag{37}$$

For any fixed L value, n exceeds m by this amount. Then from (36)

$$\nu_p = f_{m+L} - f_m = \frac{\theta_{m+L}}{T} - \frac{\theta_m}{T} = \frac{\Delta_{L, m}}{T} \tag{38}$$

where θ, Δ are defined in (1) and (2).

13

It has been shown previously in (3) that the $\Delta_{L,m}$ set contains no repeated terms for a fixed L. Thus at the fixed delay x = L, each sidelobe term peaking on this line will do so at its own unique frequency as given by (38). Since this logic holds for any and all delay values L, it may be seen that all ϕ_{nm} peaks involve only one term of the second sum of (23). The ϕ_{nm} peaks will be spaced by integral values in both x and y.

While these peaks do not coalesce, their density of distribution is not uniform. There are exactly N-L peaks at delay $\tau = \pm$ LT. At unit delay there are N-1 peaks and at delay $\tau =$ (N-1) T there is but one peak. An equivalent argument may be made by reversing delay and frequency roles. At frequency $\nu = \pm$ L/T there are exactly N-L peaks over the complete τ span for this frequency. Thus the area near the origin tends to be rather busy so that the technique is almost a counter example of Green's Theorem[6,7], as indicated in the next paragraph. (Green conjectured on the maximum amount of area near the main lobe that could be kept completely free of sidelobe volume.)

Each ϕ_{nm} peak has a region of influence which is constrained absolutely to a span 2T units wide in the delay direction. This τ cutoff results from the limited pulse duration T. The region of influence in the frequency direction of each ϕ_{nm} is not similarly constrained. The behavior of each sidelobe peak is essentially that of ϕ_{nm} of (21) with τ, ν measured from peak center. The behavior in frequency is of the sin z/z form. Thus each peak has a "channel" of influence of width 2T in delay. This influence decays to zero at the channel delay boundaries and drops off as sin z/z in the frequency direction. These channels of influence explain why the ν axis ($\tau = 0$) is completely clear of pedestal (cross product) effects and why the τ axis ($\nu = 0$) is never free from these terms.

The overlapping of the ϕ_{nm} sidelobe terms produces reinforcement and cancellation effects which are quite complex because of the amplitude and phase relationships involved. However certain locations in the pedestal region will have predictable values. Along any delay ridge line $\tau = \tau_p$ as per (36) the delay argument of ϕ_{nm} of (23) will be zero. We may now use (19) to obtain

$$\phi_{nm}(0, \nu) = \frac{\sin\pi\left(f_n - f_m - \nu\right)T}{\pi\left(f_n - f_m - \nu\right)T} \qquad (39)$$

now let

$$\nu_r = \pm \frac{r}{T} \qquad (40)$$

14

where r is any integer. The angle β of the $\sin \beta / \beta$ function of (39) becomes [see also (4)].

$$\beta = \pi \left[\frac{\theta_n}{T} - \frac{\theta_m}{T} + \frac{r}{T} \right] T = \pi \left(\theta_n - \theta_m + r \right) \tag{41}$$

Clearly (39) will then be zero for all $\beta \neq 0$ and will be unity only for $\beta = 0$. So with the normalization implied by (23) it may be stated that in the sidelobe region, for all integer coordinate pairs of the normalized delay (x) and frequency (y), the $| X |$ function will either be zero or 1/N.

There is an orthogonality effect at work here between ϕ_{nm} terms belonging to a delay channel. Each ϕ_{nm} center occurs at the zeros of all other ϕ_{nm} tails in that channel. Thus the sidelobe values are constrained at a set of points to be either 1/N or zero in value. Even though the sidelobe values are "anchored" at N (N-1) points, the actual peak values in the pedestal exceed 1/N. The area under these peaks appears to be quite small. This situation will be demonstrated in the presentation of numerical data which follows.

NUMERICAL RESULTS

The building block of the burst waveforms considered here is the simple CW pulse. The ambiguity surface for a CW pulse may be obtained by setting N = 1 in (23) and using (21) to obtain

$$\left| \chi \ (x,y) \right| = \left| (1 - |x|) \ \frac{\sin \pi y \ (1 - |x|)}{\pi y \ (1 - |x|)} \right| \tag{42}$$

where x is normalized delay (τ/T) and y is normalized frequency (νT). At zero doppler (y = 0) a cut along the delay axis would show a triangle of unit height at x = 0 and two-unit base extending from x = -1 to x = +1. At zero delay (x = 0) a $\left| \sin \pi y / \pi y \right|$ behavior would result. A "3-D" view of this surface is shown in Figure 1. The "viewer" is positioned out on the +x axis and is looking toward the origin. Successive frequency "cuts" at different delay values are calculated and plotted with successive y-offsets. The plotter pen is lifted when a previous cut surface obscures view, thus creating a "3-D" effect. (The writer is indebted to Dr. L. W. Bauer for this very useful software.) The vertical scale on the right pertains to the first cut (which is everywhere zero in this case). The vertical scale for the last cut starts at the tic mark above the word "DELAY" on the left vertical axis and extends to the top line of the chart box. These plots are useful in presenting an overall picture of the detection process. For precise quantitative work $\left| \chi \right|$ versus x or y plots will be employed.

Figure 2 shows a portion of the ambiguity surface for a 10-pulse QFM burst in which each successive pulse has a 1/T Hz frequency offset from the previous pulse. The classic FM-ridge is clearly in evidence and contains most of the volume under the surface. Note that the range and doppler resolution of the ridge changes with delay. At large delays only a few pulses are effectively combined so that the resulting time-bandwidth product of the process is low. More pulses become involved as x approaches zero and the ridge shows a corresponding narrowing in x and y. Figure 3 presents a somewhat different perspective of the same surface.

Figure 4 shows the ambiguity surface for a 10-pulse code derived from Welch's theorem using p = 11 and g = 2. Since the volume under the $\left| \chi \right|^2$ surface must equal unity, a change from QFM to the Welch pattern spreads the FM ridge volume out over the pedestal region. The difference triangle of Table 1 predicts a sidelobe at delay x = 9 and frequency y = -1. This peak may be clearly seen near the front of Figure 4. At delay 8 peaks at y = -3 and +4 are predicted and are clearly visible. At delay 7 peaks at y = -7, 1 and 2 are
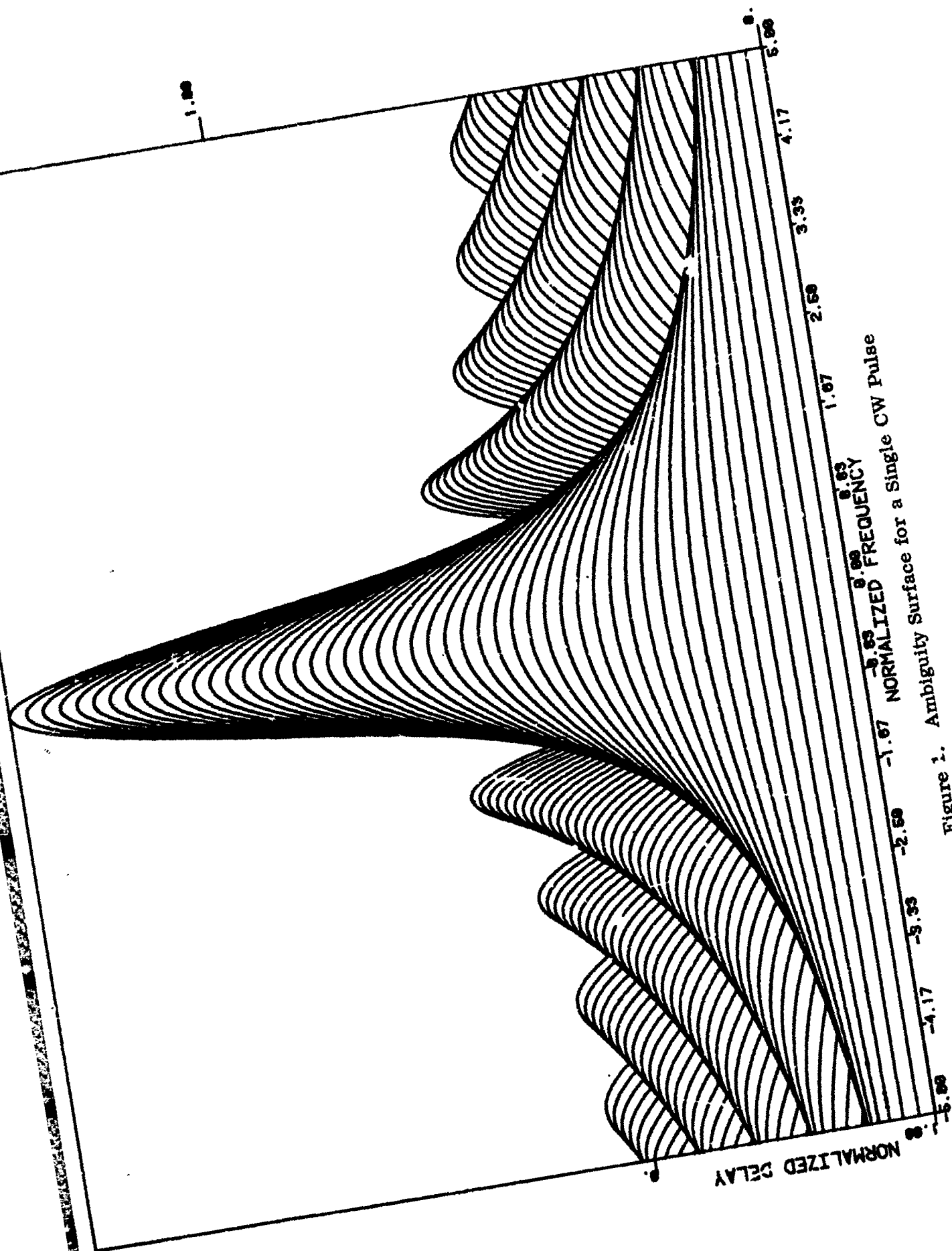
Figure 1. Ambiguity Surface for a Single CW Pulse

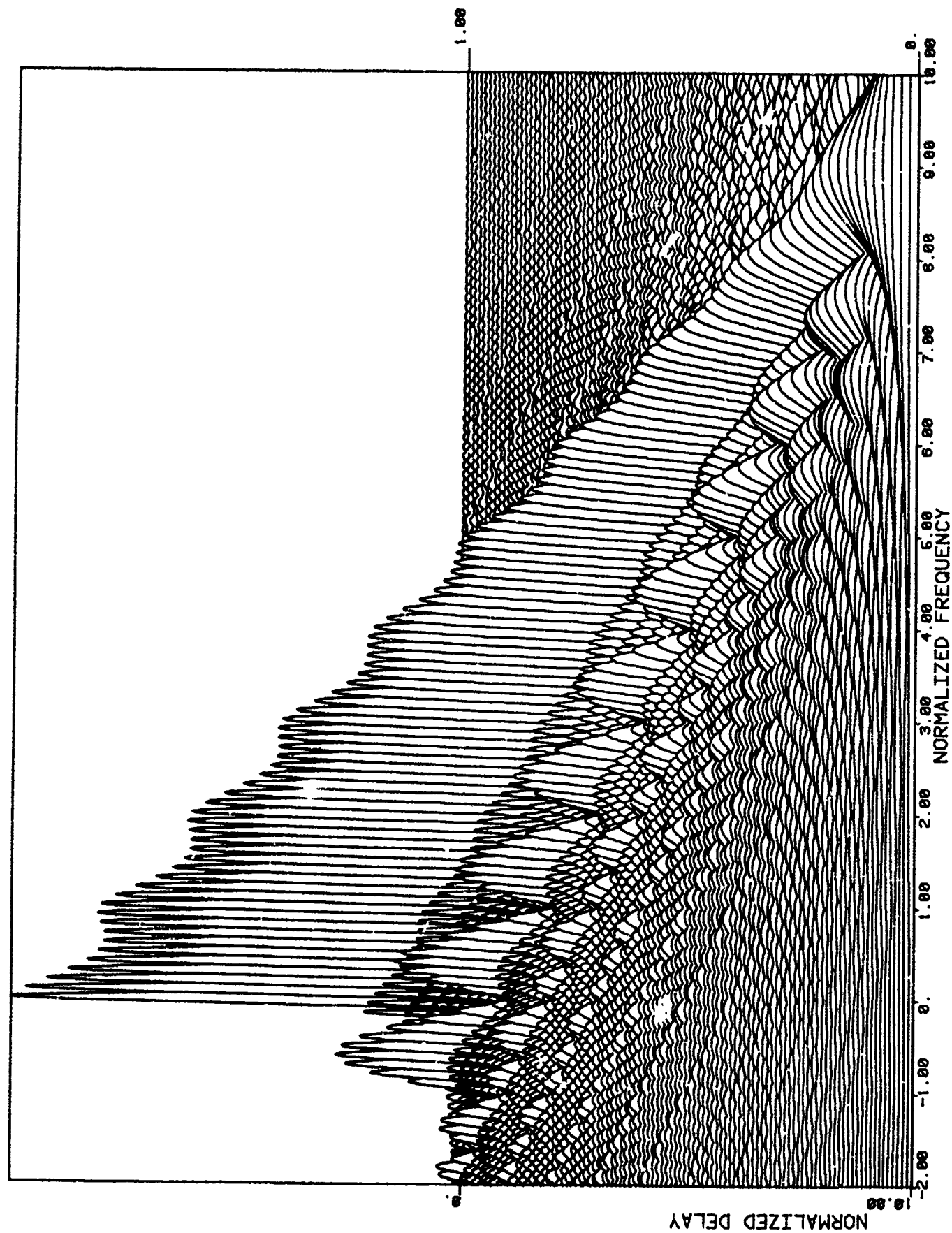NORMALIZED FREQUENCY

NORMALIZED DELAY

18

Figure 2.   Ambiguity Surface for a 10-Pulse QFM Burst
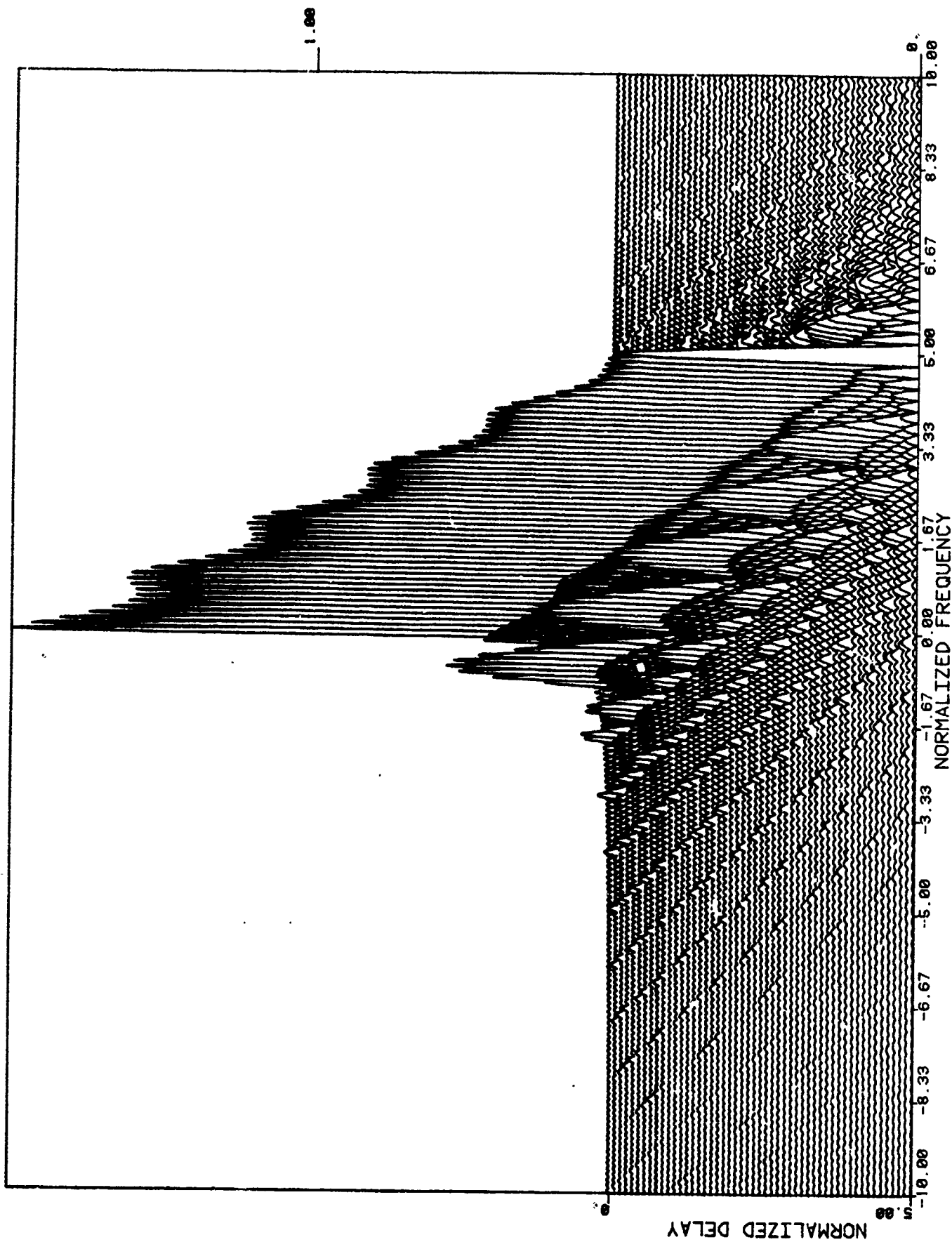
NORMALIZED FREQUENCY

NORMALIZED DELAY

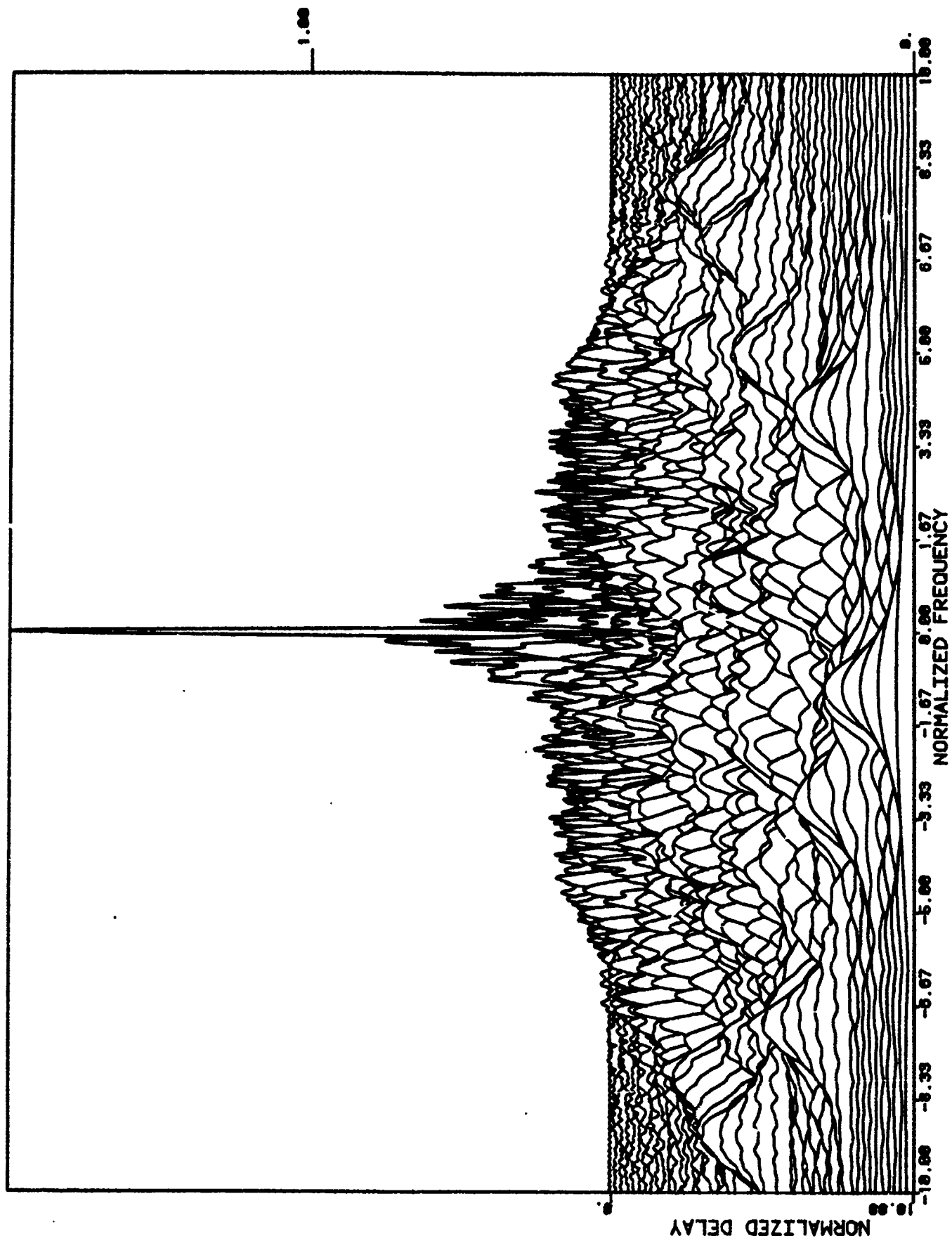19

Figure 3. Ambiguity Surface for a 10-Pulse QFM Burst

20

Figure 4. Ambiguity Surface for the Welch–10 Code (p = 11, g = 2)

21

indicated by Table 1. The peak at -7 may be seen in Figure 4 but the peaks at 1 and 2 coalesce and are not obvious. As the delay gets smaller more peaks exist per delay-axis cut and overlap effects mask the basic form of the individual peaks.

Figure 5 shows the same data as Figure 4 without the successive y-axis offsets used to emphasize the "3-D" effect. As a result all constant-delay frequency plots are referenced to the baseplane and pedestal peaking effects are accurately displayed. The tendency for side-lobe spiking above the 1/N level due to ϕ_{nm} term overlaps near the origin is evident in this figure.

The doppler axis response for x = 0 is shown in Figure 6. As was predicted from (29) and associated discussion a sin z/z behavior is seen here with the zero of the mainlobe occurring at y = 0.1 = 1/N. Note that this behavior continues without end in the y dimension.

Figure 7 shows the delay axis response for y = 0. From x = 0 to x = 1 the sin Nz/ (N sin z) functional as described in the discussion of (35) is operative along with spillover from the pedestal ϕ_{nm} terms. Beyond x = 1 the ϕ_{nn} terms vanish and only the ϕ_{nm} pedestal terms of (23) are operative. Since no ϕ_{nm} peaks occur on the x axis, the response will be zero on this axis for all integral values of x as was discussed following (41). Figure 7 corroborates this conclusion.

The worst sidelobe peak was measured as 0.21 which 2.1 times the (normalized) ϕ_{nm} term peak value. The general neighborhood of this peak is shown in Figure 8. It appears that random phasing of the ϕ_{nm} sidelobes can produce isolated peaks of the order of 6-dB over the 1/N value.

The Welch-30 code for p = 31, g = 3 is considered next. It was shown earlier that if x, y are restricted to integer values, the pedestal region will be either zero or 1/N depending on the nonexistence or existence of a ϕ_{nm} peak at the x, y coordinate. Figure 9 shows a 3-D plot restricted to integer x and y values. The sidelobe peaks as well as the main peak for this code are clearly displayed by this plotting artifice. Triangles indicate isolated peaks while the flat-topped sections indicate two or more frequency-adjacent peaks. The increasing density of peaks with reduction of delay is quite evident from this figure.
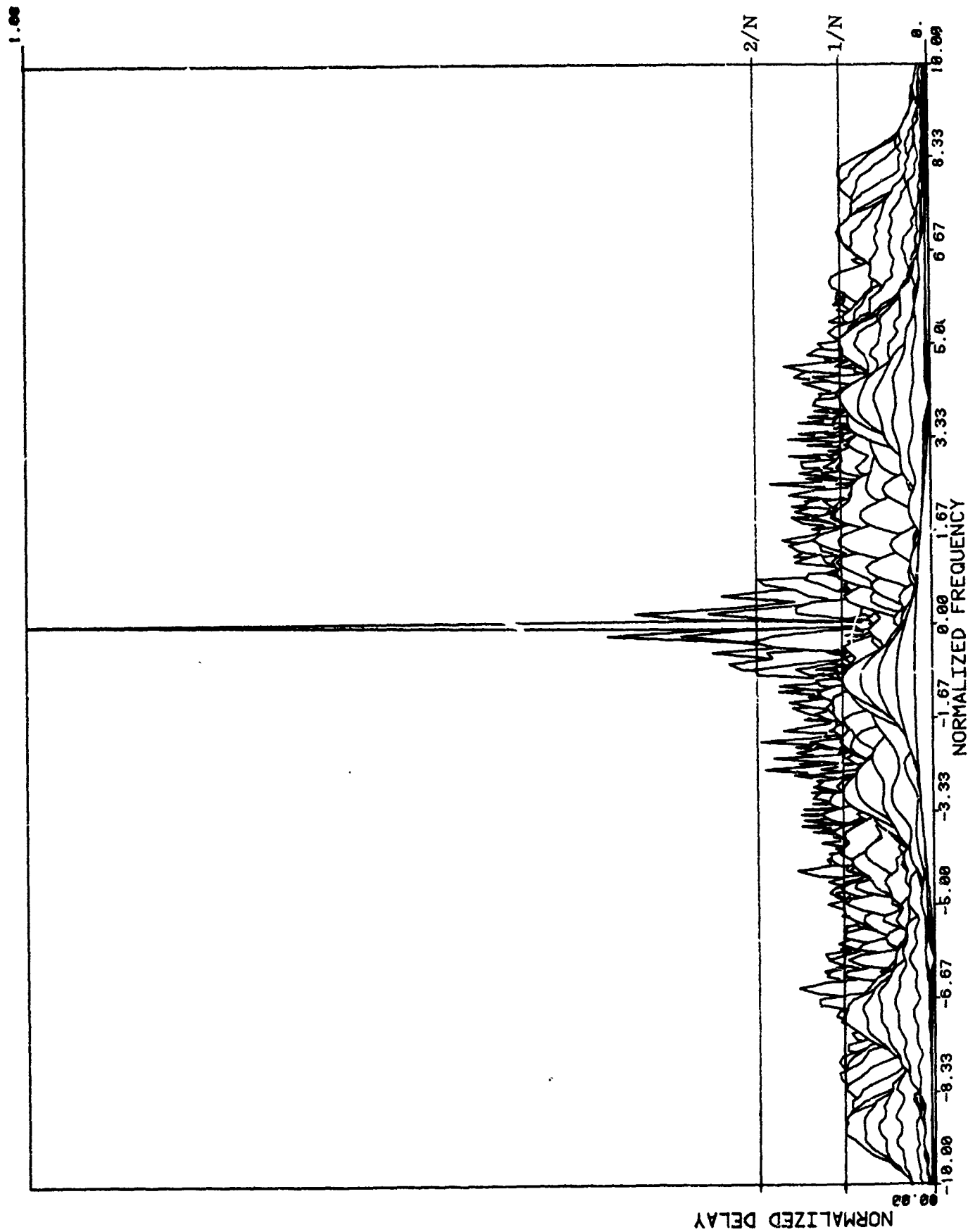
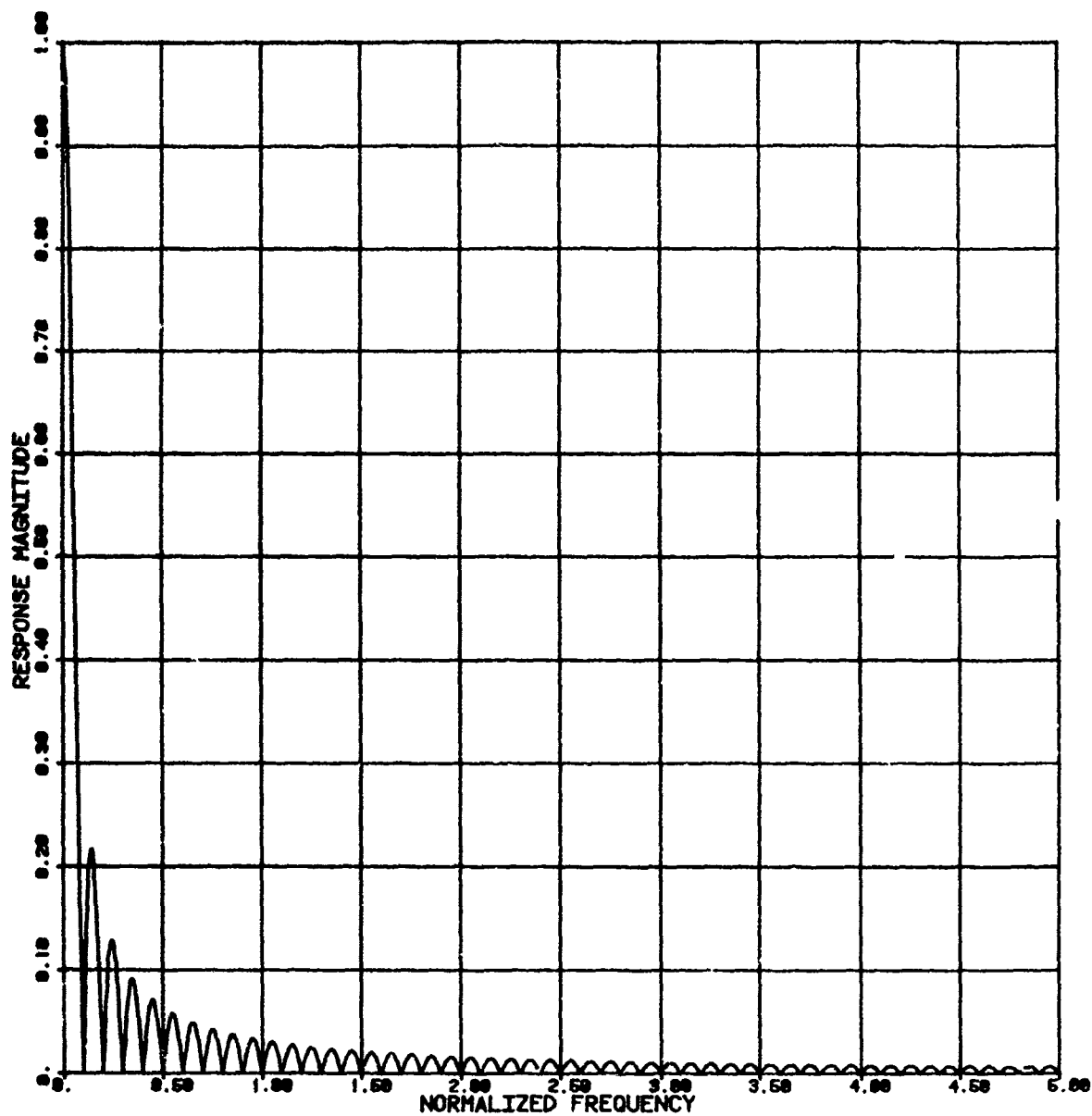Figure 5. Welch-10 Ambiguity Surface, Zero-Offset Presentation

NORMALIZED FREQUENCY

NORMALIZED DELAY

23

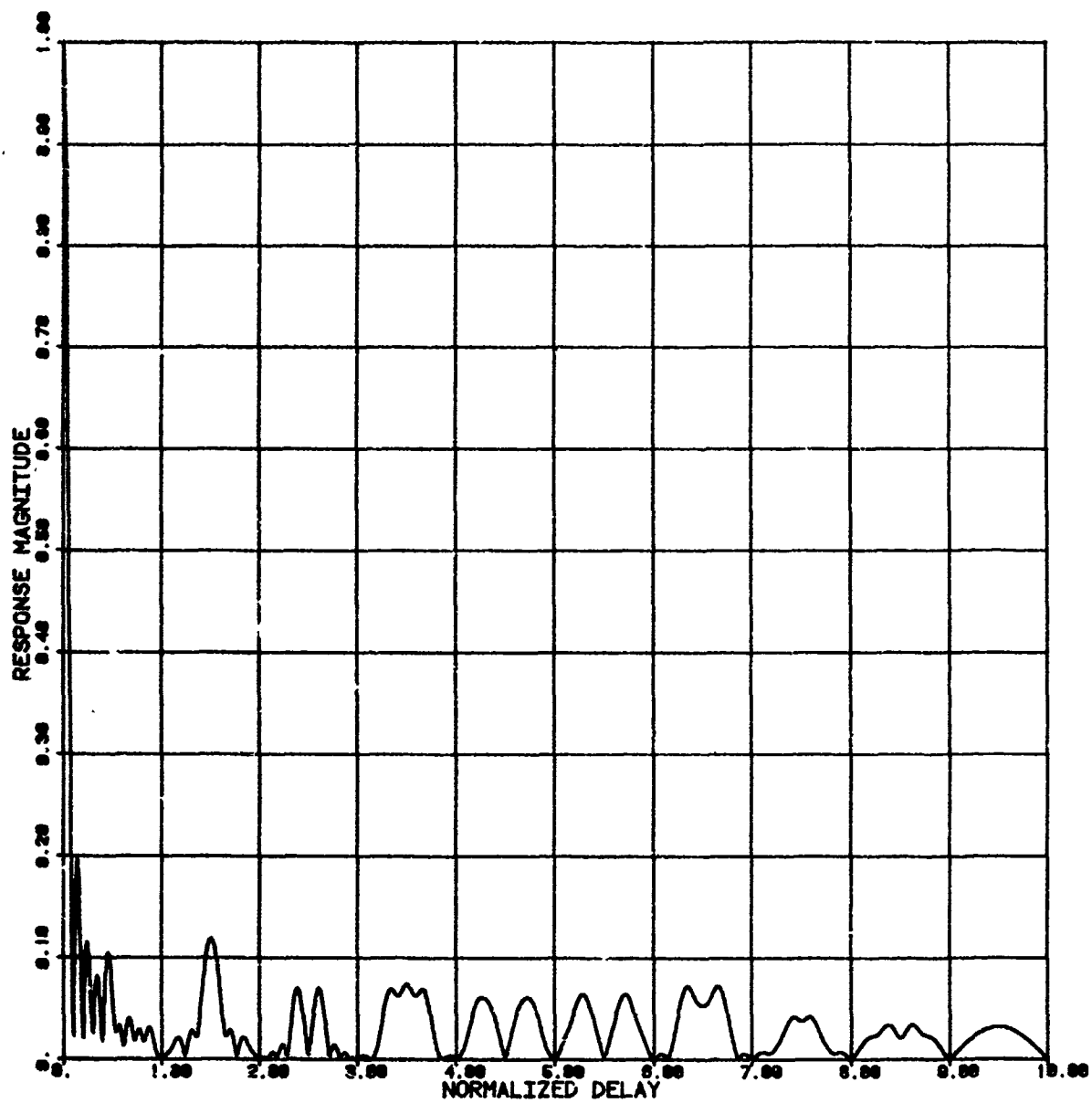Figure 6. Frequency Axis Response for x = 0 for the Welch-10 Burst

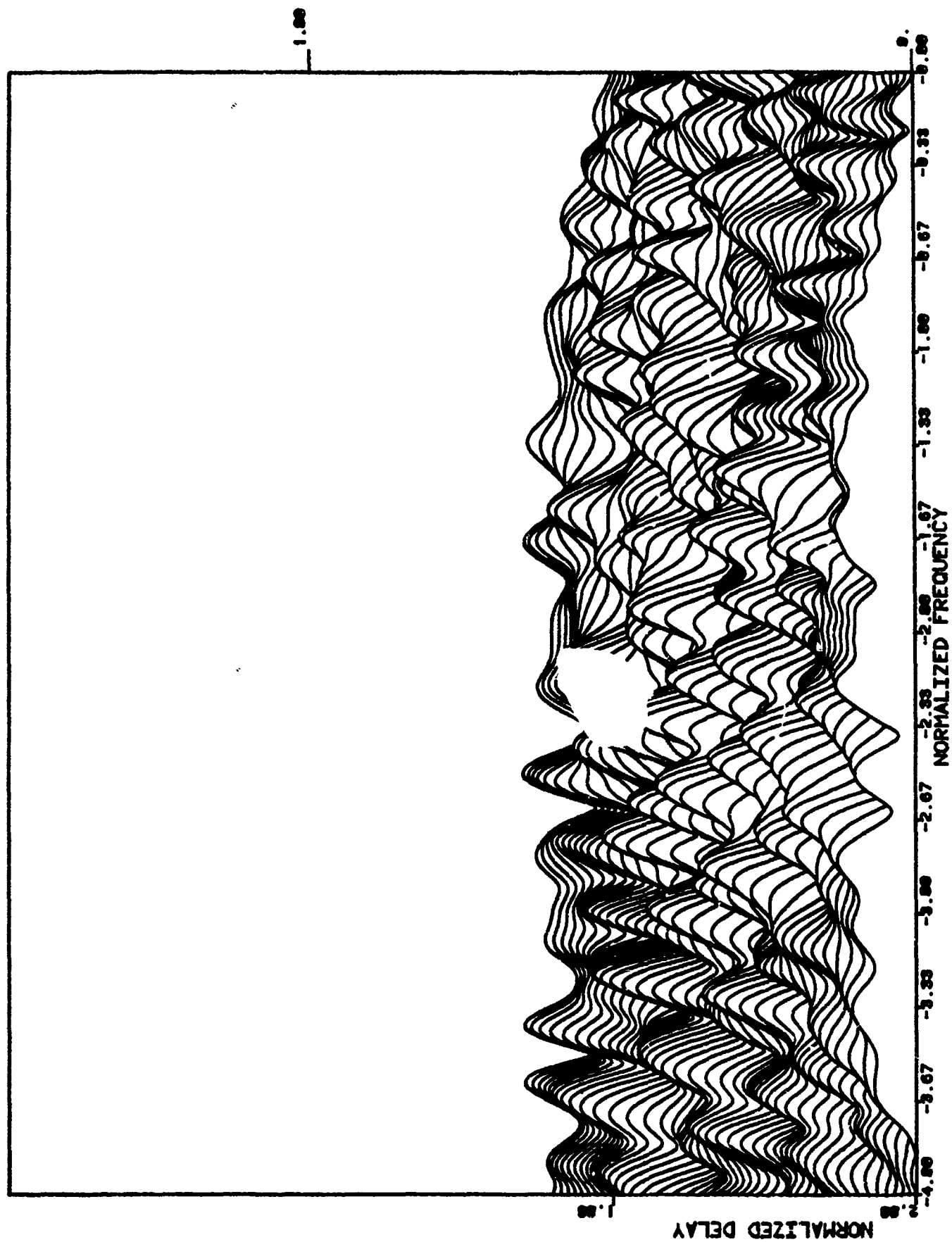Figure 7. Delay Axis Response for y = 0 for the Welch-10 Pulse Train

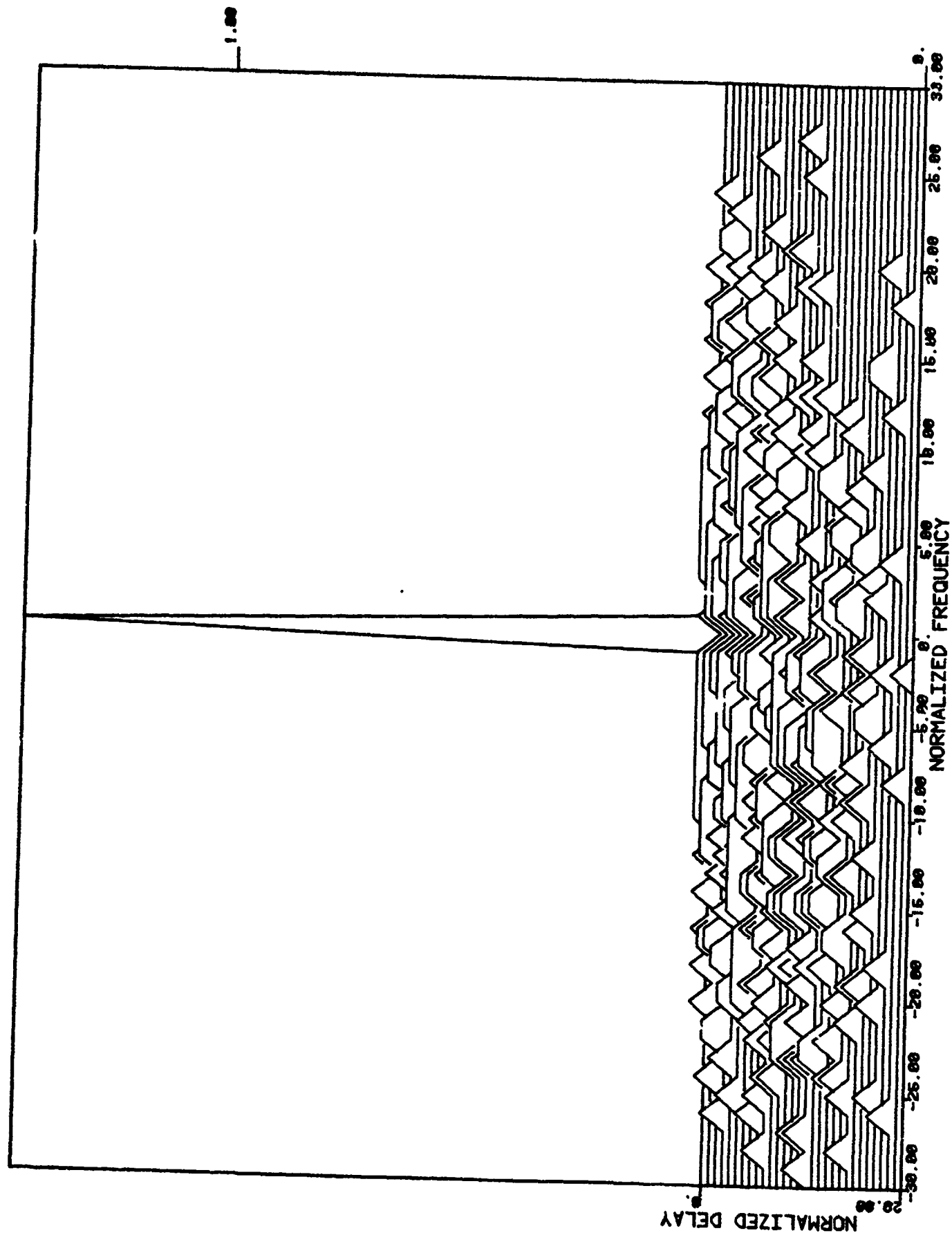Figure 8. Pedestal Region Near the Highest Peak for the Welch-10 Pulse Train

Figure 9. Welch-30 Pulse Code Evaluated at Integer x, y Values Only

27

Figure 10 is a zero-offset 3-D plot of the Welch-30 ambiguity surface which shows peaks in true perspective. Pedestal spiking above 1/N near the origin is evident. Comparison with Figure 5 would indicate that pedestal peak levels do vary inversely with N with 2/N representing a fair estimate of the largest pedestal peak. There does not appear to be any theoretical bar to the use of arbitrarily large N values.

Figure 11 shows the doppler axis cut for the 30-pulse code. As expected a sin z/z frequency behavior is evidenced with the first zero at y = 1/30. Figure 12 shows the delay axis cut out to x = 1. The first zero here is at x = 1/30 as expected. The complete positive delay region for y = 0 is shown in Figure 13. The main peak is obscured by the choice of the x-axis scale. The sidelobes are very well behaved, with relatively few sharp excursions above the 1/N value.

Figure 14 is a frequency cut taken at a delay of x = 25. The 25th row of the difference triangle for this Welch-30 sequence predicts sidelobe peaks at y = -25, -20, 2, 14 and 15. These locations are clearly confirmed by Figure 14. Note that the isolated ϕ_{nm} terms have exactly the peak value 1/N while the two peaks at y = 14, 15 create mutual interference effects which result in a small spike which exceeds the 1/N value.

Figure 15 shows a frequency cut taken closer to the main peak, at x = 5. The mutual interference effects from groups of frequency-adjacent ϕ_{nm} peaks are clearly evident near the center of this plot. The highest peak found for this waveform was at delay x = 1.4 and had a value of 0.078. Figure 16 shows a frequency cut at this delay with the peak in question showing near y = 3.

The ambiguity surface taken for a region near this peak is shown in Figure 17. At the front of this plot is a frequency cut taken at delay x = 3. Note that there are ϕ_{nm} peaks at y = 4, 6, and 7 and no ϕ_{nm} peak at y = 5. In spite of the gap at y = 5 the mainlobe regions of the peaks at 4 and 6 are highly distorted indicating significant overlap effects from the many (27) ϕ_{nm} peaks which fall at this delay. The rapid undulations of this surface are to be compared with equivalent data taken for the Welch-10 burst in Figure 8. Note also the lower level of the Figure 17 data as compared to Figure 8. Increasing the pulse count from 10 to 30 has increased range and doppler resolution by 3 to 1 and has lowered the sidelobe height by about the same ratio.
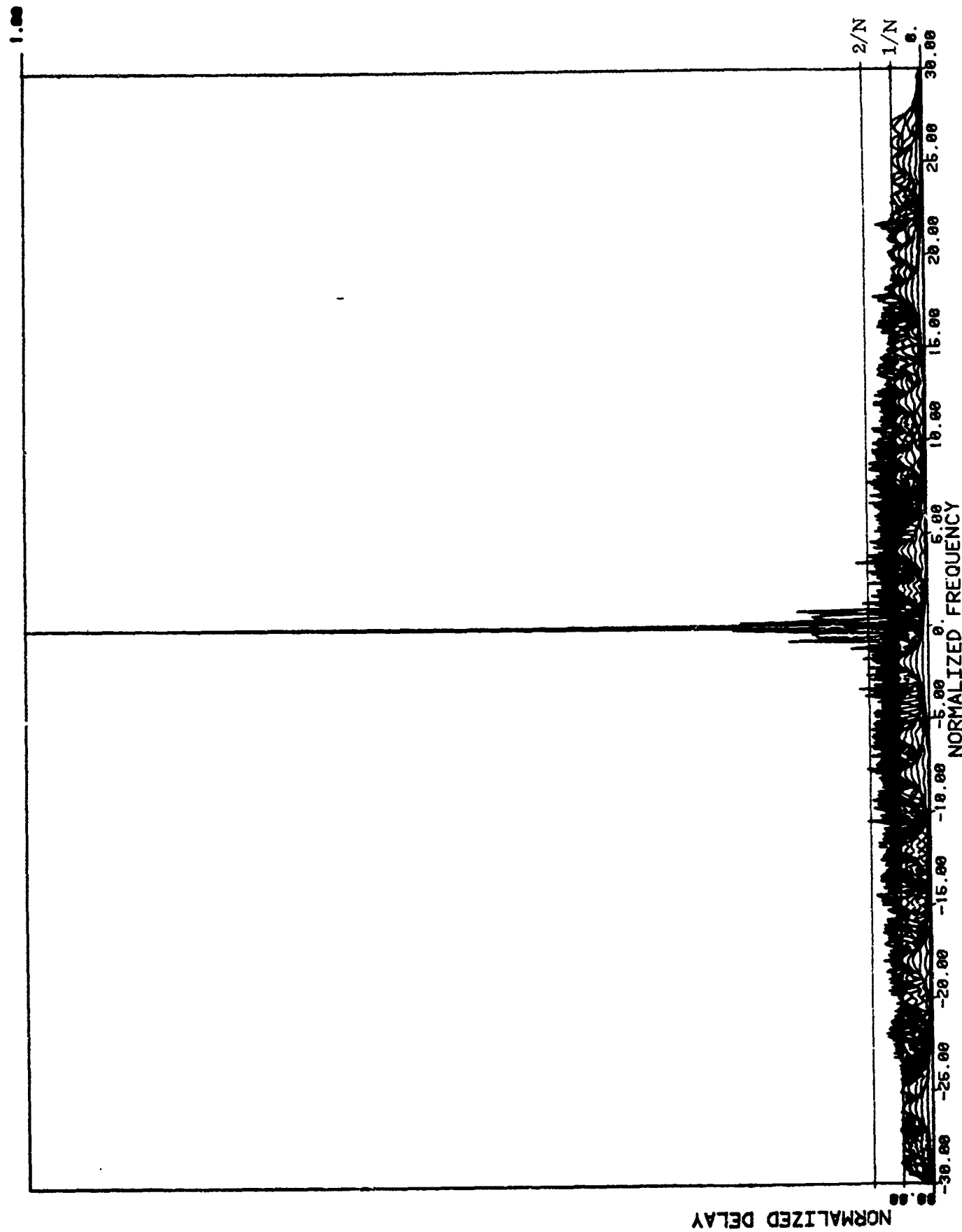
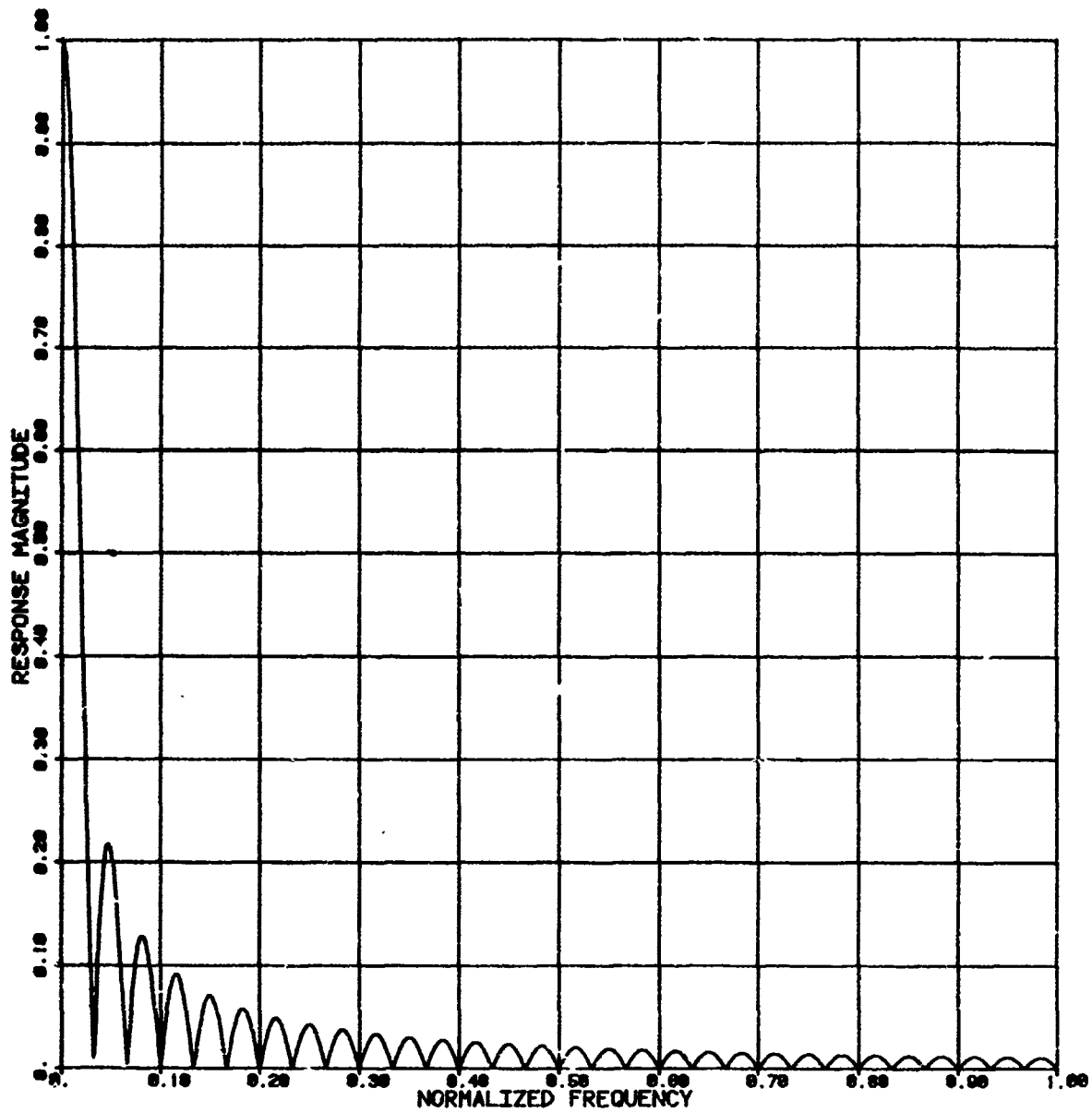Figure 10. Welch-30 Ambiguity Surface, Zero-Offset Presentation

29

Figure 11. Frequency Axis Response for x = 0 for the Welch-30 Pulse Train
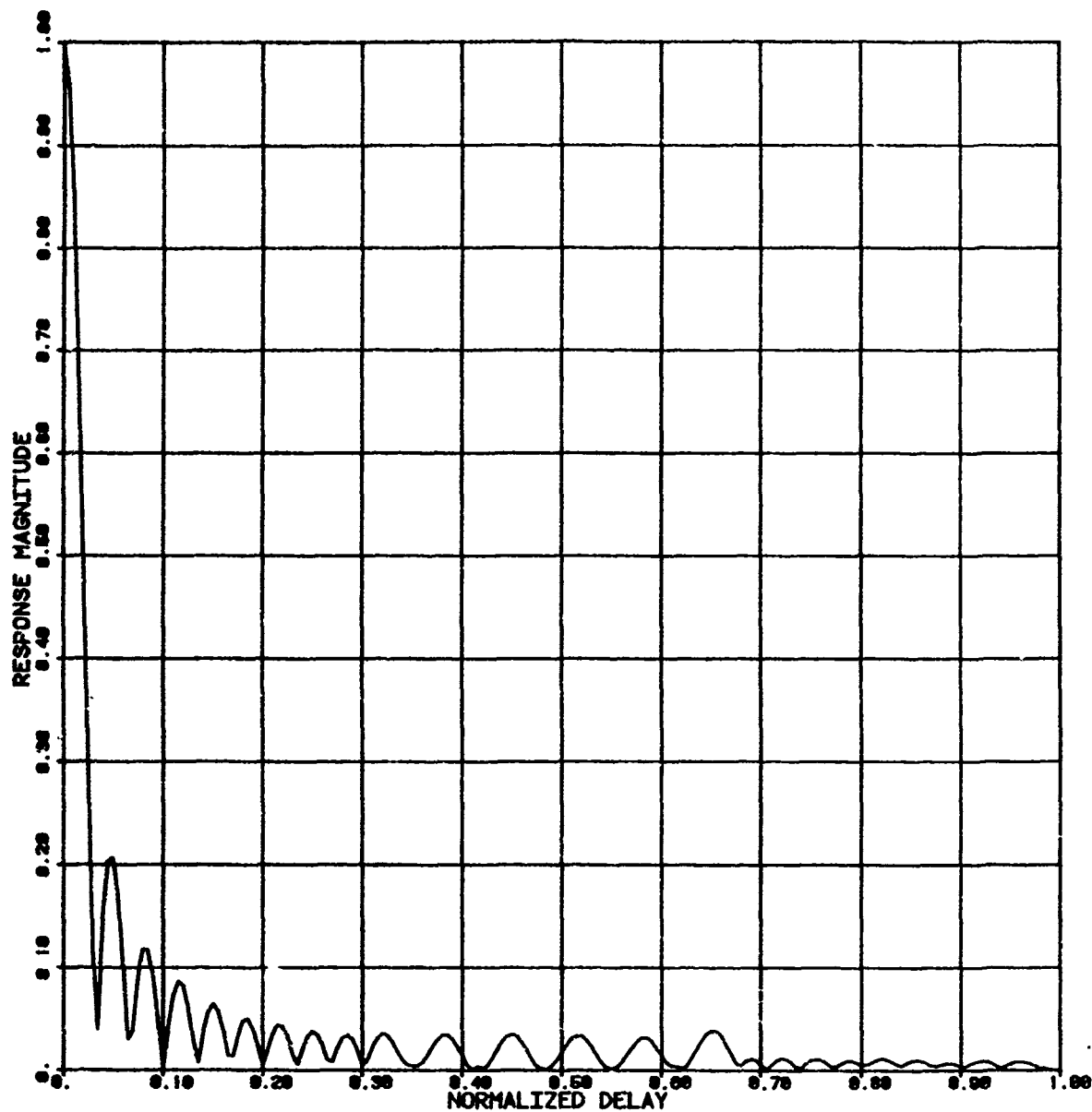
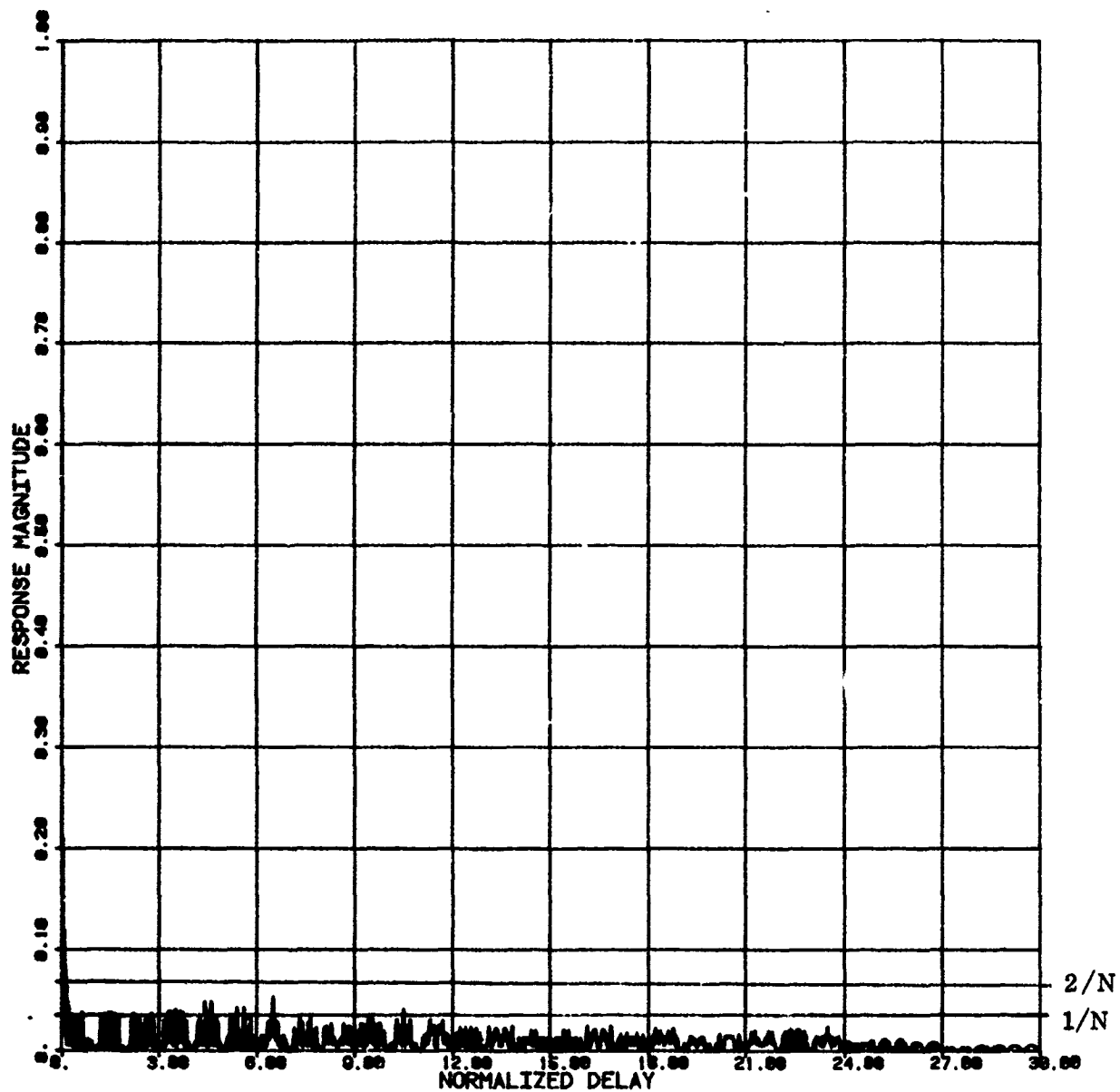Figure 12.   Delay Axis Response for y = 0 for the Welch-30 Pulse Train

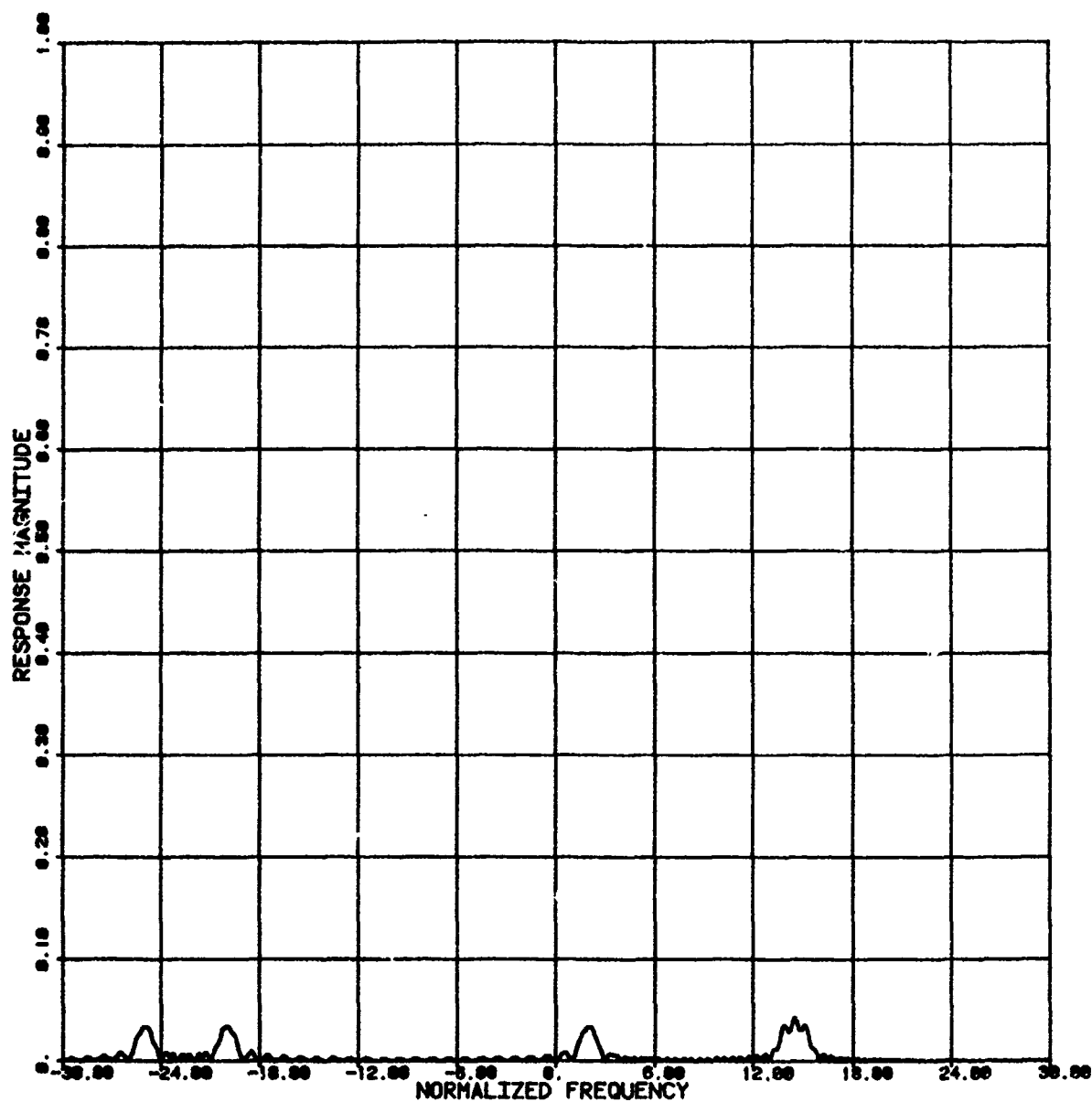Figure 13.   Complete Delay Axis Response for the Welch-30 Code at y = 0

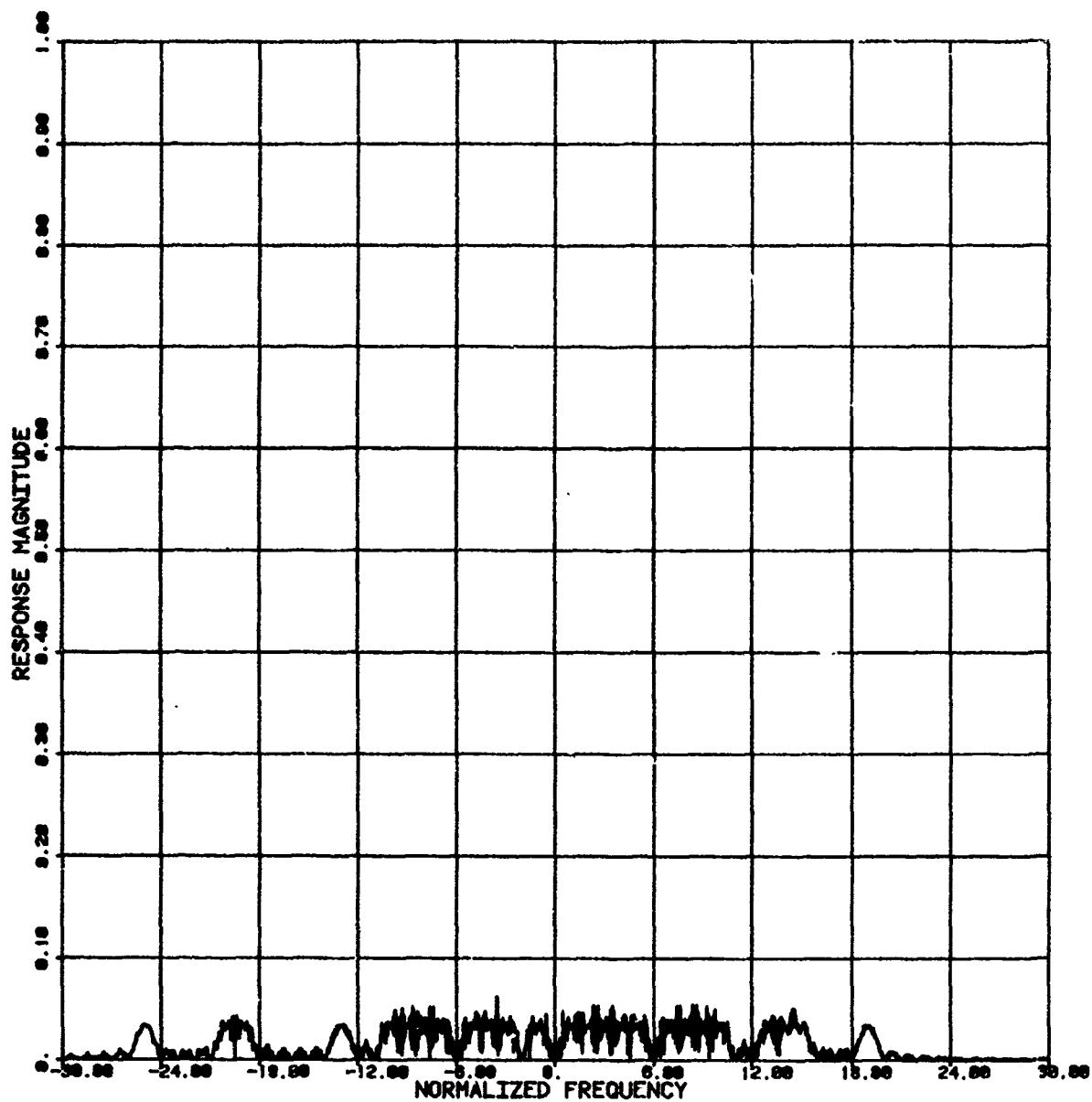Figure 14. Frequency Cut at x = 25 for the Welch-30 Burst

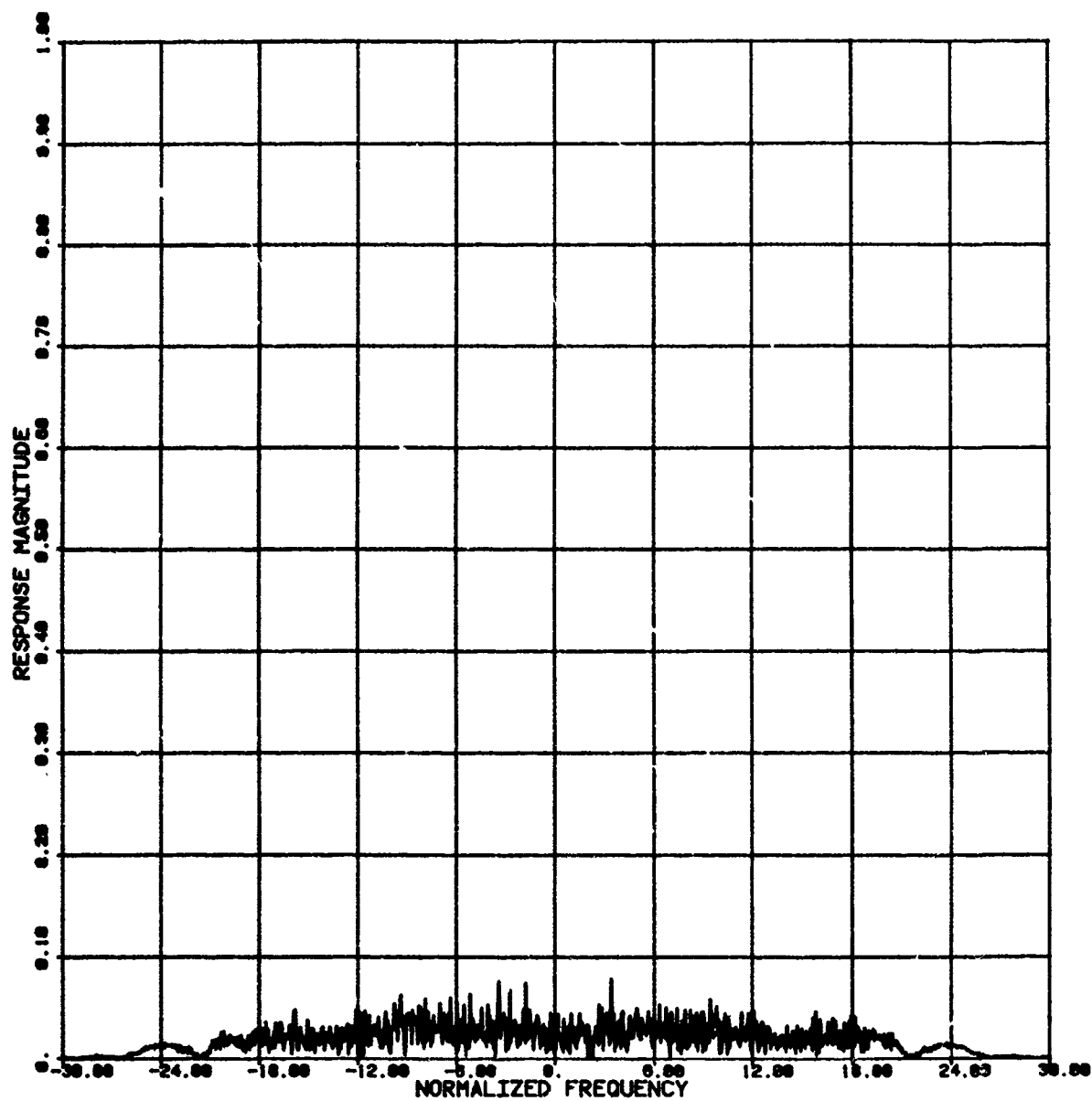Figure 15.   Frequency Cut at x = 5 for the Welch-30 Burst

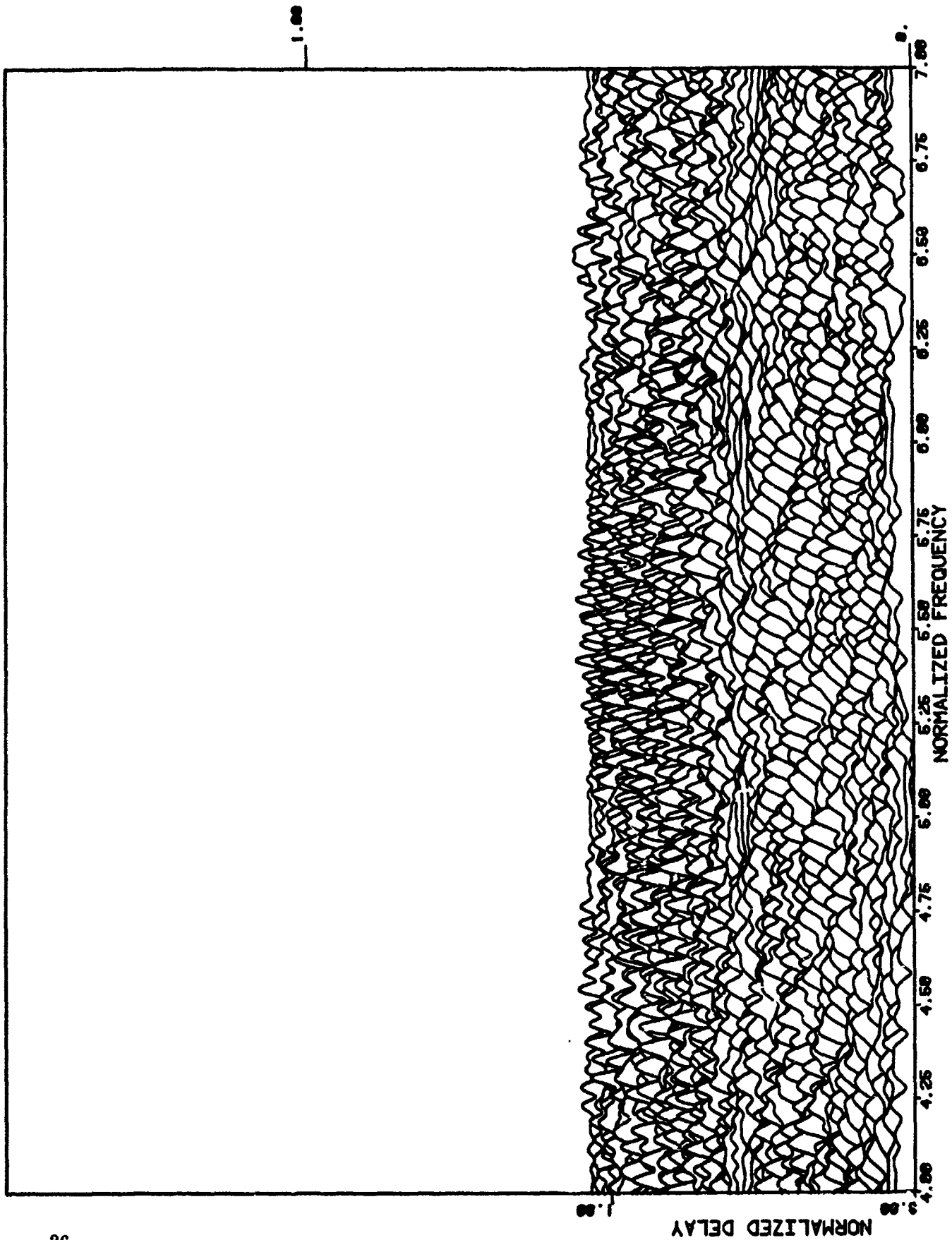Figure 16. Frequency Cut at x = 1.4 for the Welch-30 Sequence

Figure 17. Ambiguity Surface in a Pedestal Region of High Activity, Welch-30 Burst

SUMMARY AND CONCLUSIONS

When the frequency-time pattern of a pulse train corresponds to one of the patterns of the special permutation matrices described, the basic pedestal components are denied location coincidences throughout the sidelobe region, thereby minimizing the peak noncentral response. Specification of the frequency channel spacing to be equal to the reciprocal of the pulse length prevents ambiguities along the delay axis so that the resulting central peak provides good resolution in both delay and frequency.

The peak pedestal level varies from $1/N$ away from the origin to $2/N$ near the central peak. This method of waveform design can be extended to arbitarily large time-bandwidth (N^2) products.

Further refinement of this basic technique might involve weighting over the pulse train for both transmit and receive. Modification of the individual pulse envelope and phase characteristics could also be considered for creation of more suitable ambiguity surfaces. None of these variations were addressed here. Such extensions of the technique for sidelobe modification must be done carefully so that the integrity of the main response is maintained.

REFERENCES

1. J.P. Costas, "Medium Constraints on Sonar Design and Performance," GE Co., Class 1 report, R65EMH33, Nov, 1965. A synopsis of this report appeared in the Eascon Convention Record, 1975, pp 68A-68L.

2. R. Price and P.E. Green, Jr., "Signal Processing in Radar Astronomy-Communication via Fluctuating Multipath Media," Lincoln Laboratory Technical Report No. 234, October, 1960.

3. S.W. Golomb and H. Taylor," Two-Dimensional Synchronization Patterns for Minimum Ambiguity," IEEE Trans on Information Theory, Vol IT-28, No. 4, July, 1982.

4. S.W. Golomb, "Algebraic Constructions for Costas Arrays," Journal of Combinatorial Theory, Publication expected early in 1984.

5. A.W. Rihaczek, "Radar Resolution Properties of Pulse Trains," Proc. IEEE, Vol 52, pp 153-164, February, 1964.

6. R. Price and E.M. Hofstetter, "Bounds on the Volume and Height Distributions of the Ambiguity Function, IEEE Trans on Information Theory, pp 207-214, April, 1965.

7. R. De Buda, "An Extension of Green's Condition to Cross-Ambiguity Functions," IEEE Trans on Information Theory, Vol IT-13, No. 1, pp 75-81, January, 1967.